Phase noise effects on phase-sensitive OTDR sensors using optical pulse compression

Alayn Loayssa, *Senior Member, IEEE,* Mikel Sagues, and Avishay Eyal, *Senior Member, IEEE*

***Abstract*—We introduce a detailed theoretical, numerical, and experimental study of the effects of laser's phase noise on the performance of phase-sensitive optical time-domain reflectometry (ϕ-OTDR) sensors that use optical pulse compression (OPC). Pulse compression is a technique that can be used to improve the received signal amplitude by increasing the effective energy of the pulses that are launched into the fiber without degrading the spatial resolution of the measurements. Therefore, it is a valuable tool to extend the range of these sensors and mitigate fiber attenuation constraints. However, it has been observed that the limited coherence of the laser source has a degrading effect on the actual performance enhancement that this method can provide. Here, we derive a theoretical model that can be used to quantify this degradation for any type of OPC such as those based on either linear frequency modulation (LFM) pulses or perfect periodic autocorrelation (PPA) bipolar bit sequences. The model facilitates numerical estimation of the sensitivity of the ϕ-OTDR measurements. It also produces theoretical expressions for the mean and the variance of the phase-noise perturbed backscatter response. These results are validated via numerical simulations and experiments in ϕ-OTDR setups using LFM as well as PPA OPC. Furthermore, we demonstrate the use of the model to investigate the basic trade-offs involved in the design of OPC ϕ-OTDR systems.**

***Index Terms*—Phase Noise, Distributed Acoustic Sensing, Optical Pulse Compression, Optical Time Domain Reflectometry, Linear Frequency Modulation, Perfect Periodic Autocorrelation Codes**

I. Introduction

DISTRIBUTED vibration sensing (DVS), also known as Distributed Acoustic Sensing (DAS), is a fiber optic sensor technology that has received considerable attention in later years due to its wide range of applications in a variety of fields such as structural health monitoring, seismic sensing, intrusion detection or in traffic monitoring [1]. These sensors are based on taking advantage of Rayleigh backscattering within either time-domain or frequency-domain reflectometric schemes; with the former being used mainly for long-range applications and the latter when the spatial resolution of the measurement is paramount.

Time-domain DVS are usually called phase-sensitive optical time-domain reflectometer sensors (ϕ-OTDR) as their use of narrowband optical sources leads to interference effects in which the phase of the optical field plays a fundamental role. There are several versions of ϕ-OTDR sensors depending on the method they use to perform the measurement [1]. The simplest is purely intensity-based and works by detecting changes in the amplitude of the backscattered signal from a particular position in the fiber as a result of excitations that alter the optical path lengths (OPL) of the interfering signals reflected by scattering centers that are illuminated by the propagating pulse. However, this provides a highly nonlinear measurement that makes it difficult to quantify the actual excitation in the fiber. Other methods are based on using coherent detection to demodulate the full optical field (amplitude and phase) of the backscattered signals. Then, the differential phase measurements between close locations in the fiber separated by the so-called gauge length provide quantified information of the OPL change between those positions due to external excitation. Finally, there is yet another kind of methods that are based on using the dependence on wavelength of the interference from the signals coming from a particular location in the fiber. These can work by directly changing the wavelength of the interrogating pulses launched into the fiber [2][3] or by using chirped pulses in which the wavelength dependence of the interference is translated to a time dependence [4]. In either case, the excitation affecting the fiber can be quantified by the shift that it induces in the interference pattern.

All these methods are based on launching interrogating pulses into the fiber. Hence the main constraint to the range of DVS systems implementing them is fiber attenuation. It makes the signal coming from far away locations in the fiber extremely weak and compromises the sensitivity of the measurement. The peak power of the pulses that can be used is constrained by the onset of nonlinear effects, particularly modulation instability. Hence, in principle, the only way to get higher power signals from remote locations is to increase the duration of the pulses. However, this would compromise the spatial resolution of the measurement. The use of optical pulse compression (OPC) relaxes this trade-off between spatial resolution and measurement sensitivity. Pulse compression has been used for years in other fields such as radar and it has also recently been applied to ϕ-OTDR sensors [5], [6], [7], [8], [9], [10], [11]. Its basic idea is to inject into the fiber signals with long durations (high energies) and high time-bandwidth products so that they can be processed upon reception with matched filters to produce narrow effective pulse widths. In its application to ϕ-OTDR, several different signal types have been used such as: linear frequency modulation (LFM) pulses [5], [7], [9], Golay codes [10] or perfect periodic autocorrelation (PPA) codes [12], [11], [13].

In principle, the measurement signal-to-noise ratio (SNR)

A. Loayssa and M. Sagues are with the Institute of Smart Cities, Electrical, Electronic, and Communications Engineering Department, Universidad Pública de Navarra, Pamplona 31006, Spain e-mail: alayn.loayssa@unavarra.es.

A. Eyal is with the School of Electrical Engineering, Faculty of Engineering, Tel Aviv University, Tel Aviv, Israel

enhancement provided by OPC in ϕ-OTDR sensors is proportional to the increased duration of the signal compared to the use of single pulses, assuming equal peak powers for both. However, such enhancement, which can be of many decibels, has not materialized in practical deployments due to the effects of the limited coherence of the sources. This limitation, induced by the phase noise of the laser in OPC ϕ-OTDR sensors, has been previously reported in several works in the literature [5], [14], [15], [16]. Its modeling, however, has been rather limited. Zou et. al. described the phase noise induced differential phase as a time-independent random variable [5]. This model fails to capture significant effects of the phase noise. In particular, it does not reflect its hindering of the matched-filtering process and the corresponding decrease in the amplitude of the processed backscatter signal. This drawback was later remedied [14] but the work only studied the average response and did not consider its variance which is critical for the measurement of dynamic signals.

In this paper, we introduce a more detailed theoretical model for the effect of the laser's phase noise on the performance of OPC ϕ-OTDR sensors. This model is tested by numerical calculations and by experimental results in ϕ-OTDR sensor setups that employ LFM as well as PPA OPC. In addition, the model is used to investigate the basic dependence of the sensor performance on the source and OPC parameters. This provides the answer to basic questions about OPC deployment such as what is the optimum sequence or pulse duration to use for a particular ϕ-OTDR sensor configuration.

II. THEORETICAL MODEL FOR PHASE-NOISE EFFECTS

A typical setup for implementing OPC ϕ-OTDR is depicted in Fig. 1. This is a conventional differential-phase OTDR sensor with homodyne detection whose implementation details are given in section IV. The light from the narrow linewidth laser source that is injected into the fiber under test is expressed as:

$$E_{\text{IN}}(t) = E(t)e^{j\phi(t)}e^{j\omega_0 t} \tag{1}$$

where $E(t)$ is a periodic complex function representing the PPA or the LFM modulations, ω_0 is the center radial frequency and $\phi(t)$ represents the laser's phase noise. The stochastic properties of $\phi(t)$ and their characterization, in narrow-linewidth laser sources, have been studied extensively in recent years [17], [18], [19], [20], [21], [22]. While these properties differ significantly from one type of laser to another, it is generally accepted that $\phi(t)$ can be modeled as a sum of terms, each with a different Power Spectral Density (PSD). The terms are commonly categorized according to the PSD of the instantaneous frequency variations which they represent. They comprise a fundamental phase noise term which represents noise with 'white' instantaneous frequency PSD and terms whose instantaneous frequency PSD's are of the form S_α/f^α with $\alpha \geq 1$. The most notable non-white term is the '1/f' or 'flicker noise' which corresponds to $\alpha = 1$. The choice of the terms that need to be included in the modeling of $\phi(t)$ depends on the type of the laser source used as well as on the time scales of interest. Generally speaking, non-white noise terms become significant when the application involves measurements over long time scales, but otherwise, the 'white' frequency PSD term may be sufficient. In this work, it was empirically found that using the simple 'white' noise term alone was sufficient for modeling the system performance with good accuracy for two very different types of lasers and for two different compression techniques. This result is attributed to the use of the differential-phase measurement approach which cancels, to some degree, the undesired slow phase variations. In accord with this finding, in all following derivations, it is assumed that $\phi(t)$ is the integral of white Gaussian noise. Namely, it is a Wiener-Levy random process whose structure function is given by: $D_\phi(\tau) = \langle[\phi(t+\tau)-\phi(t)]^2\rangle = 2|\tau|/\tau_c$ where $\tau_c = 1/(\pi\Delta\nu)$ is the laser's coherence time and $\Delta\nu$ is its linewidth [23].

In the following, we present the model that relates the output of the OPC ϕ-OTDR sensor to the input field in (1). This model facilitates the numerical characterization of the system's performance. It also produces theoretical expressions for the mean and the variance of the phase-noise perturbed backscatter response. These expressions, which as shown below can be readily verified experimentally, provide additional insight about the phase noise effects and can be used for further confirmation of the model.

In OPC-based techniques, the output of the measurement system is digitally cross-correlated with $E(t)$ to obtain the compressed response. The presence of phase noise leads to the deviation of the fiber's backscatter measurement from the nominal signal. To evaluate this deviation, it is helpful to introduce the response of the measurement system to a perfect reflector positioned at a roundtrip delay of τ_{rt}:

$$\begin{aligned} &R(\tau,\tau_{rt}) \equiv \\ &e^{j\omega_0\tau_{rt}}\int_0^T E^*(t-\tau)E(t-\tau_{rt})e^{j[\phi(t-\tau_{rt})-\phi(t)]}dt \end{aligned} \tag{2}$$

Note that it takes into account neither propagation loss, which will be introduced later, nor receiver responsivity and gain. In the absence of phase noise we have:

$$R(\tau,\tau_{rt}) = e^{j\omega_0\tau_{rt}}\int_0^T E^*(t-\tau)E(t-\tau_{rt})dt \equiv q(\tau-\tau_{rt}) \tag{3}$$

where $q(t)$ describes the autocorrelation of the transmitted signal, i.e., the nominal compressed response. Ideally, it is desired that $q(t)$ is as narrow as possible as it determines the spatial resolution of the method. The mean of the resulting response can be readily calculated as:

$$\begin{aligned} &\langle R(\tau,\tau_{rt})\rangle = \\ &= e^{j\omega_0\tau_{rt}}\int_0^T E^*(t-\tau)E(t-\tau_{rt})\langle e^{j[\phi(t-\tau_{rt})-\phi(t)]}\rangle dt \\ &= e^{j\omega_0\tau_{rt}}\int_0^T E^*(t-\tau)E(t-\tau_{rt})e^{-\tau_{rt}/|\tau_c|}\,dt \\ &= e^{-\tau_{rt}/|\tau_c|}\,q(\tau-\tau_{rt}) \end{aligned} \tag{4}$$

This article has been accepted for publication in IEEE/OSA Journal of Lightwave Technology. This is the author's version which has not been fully edited and content may change prior to final publication. Citation information: DOI 10.1109/JLT.2021.3138249

Now it is assumed that the signal in (1) is launched into an optical fiber and the backscattered light is coherently detected. By using homodyne detection, the setup yields a complex signal, $I(t)+jQ(t)$, which is digitally processed to 'compress' the code and give the measured complex backscatter profile of the sensing fiber, $\tilde{r}(\tau)$ (where $\tau \equiv 2z/v$ denotes the roundtrip time to a position z in the fiber and v is the group velocity of light in the fiber). The result is a weighted sum of compressed responses:

$$\tilde{r}(\tau) = \int_0^{T_{rt}} r(\tau_{rt}) R(\tau, \tau_{rt}) d\tau_{rt} \tag{5}$$

where T_{rt} is the round-trip delay to the end of the fiber and $r(\tau_{rt})$ is the backscatter coefficient:

$$r(\tau_{rt}) = \rho(\tau_{rt}) e^{-\tilde{\alpha}\tau_{rt}} \tag{6}$$

Here ρ is a complex white random process satisfying:

$$\langle \rho(\tau_{rt}) \rho^*(\tau_{rt}{}') \rangle = \sigma_\rho^2 \delta(\tau_{rt} - \tau_{rt}{}') \tag{7}$$

and $\tilde{\alpha}$ describes the fiber's attenuation. This measured backscatter profile, $\tilde{r}(\tau)$, is a doubly stochastic random process of time. One source of randomness is the laser's phase noise while the other is the stochastic nature of Rayleigh scattering which varies from one fiber to the other and depends on wavelength and temperature.

Given $r(\tau_{rt})$ we can calculate the mean measurement response as:

$$\begin{aligned} \langle \tilde{r}(\tau) \rangle &= \int_0^{T_{rt}} r(\tau_{rt}) \langle R(\tau, \tau_{rt}) \rangle d\tau_{rt} \\ &= \int_0^{T_{rt}} r(\tau_{rt}) e^{-\tau_{rt}/|\tau_c|}\, q(\tau - \tau_{rt}) d\tau_{rt} \\ &= q(\tau) * \left[\rho(\tau) e^{-(\tilde{\alpha} + 1/|\tau_c|)\tau} \right] \end{aligned} \tag{8}$$

where $\langle\rangle$ denotes averaging over different realizations of the phase noise and $*$ denotes convolution. Interestingly, the mean backscatter profile has the same phase as the expected profile in the absence of phase noise and the only effect of the phase noise is an increase of $1/\tau_c$ in the decay rate of the amplitude. To get additional insight to the degradation of sensing performance with distance it is also interesting to evaluate the variance of $\tilde{r}(\tau)$:

$$\sigma_r^2(\tau) = \langle |\tilde{r}(\tau) - \langle \tilde{r}(\tau) \rangle|^2 \rangle = \langle |\tilde{r}(\tau)|^2 \rangle - |\langle \tilde{r}(\tau) \rangle|^2 \tag{9}$$

Note, that here we refer to a single realization of the Rayleigh scatterers, and all averages were made over different realizations of the phase noise. Namely, it is assumed that we have a single fiber at a given temperature and the optical frequency is fixed. Hence, $\langle \tilde{r}(\tau) \rangle$ and $\sigma_r^2(\tau)$ are essentially random processes. However, since $\rho(\tau)$ is a stochastic process, which takes different realizations for different fibers, wavelengths, and temperatures, to obtain a more general result it is useful to implement also averaging over an ensemble of fibers of the same type but with different realizations of Rayleigh scatterers. We denote this type of averaging as $\langle \rangle_{\text{fibers}}$. The mean signal power will be defined as $\langle |\langle \tilde{r}(\tau) \rangle|^2 \rangle_{\text{fibers}}$ and the variance will be defined as $\langle \langle |\tilde{r}(\tau) - \langle \tilde{r}(\tau) \rangle|^2 \rangle \rangle_{\text{fibers}}$. To proceed we first calculate the mean signal power:

$$\begin{aligned} \langle |\langle \tilde{r}(\tau) \rangle|^2 \rangle_{\text{fibers}} &= \\ &= \int_0^{T_{rt}} \int_0^{T_{rt}} \langle r(\tau_{rt}) r^*(\tau_{rt}{}') \rangle_{\text{fibers}} e^{-(\tau_{rt} + \tau_{rt}{}')/|\tau_c|} \\ &\qquad \cdot q(\tau - \tau_{rt}) q^*(\tau - \tau_{rt}{}') d\tau_{rt} d\tau_{rt}{}' \\ &= \sigma_\rho^2 \int_0^{T_{rt}} e^{-2(\tilde{\alpha} + 1/|\tau_c|)\tau_{rt}} |q(\tau - \tau_{rt})|^2 d\tau_{rt} \\ &= \sigma_\rho^2 e^{-2(\tilde{\alpha} + 1/|\tau_c|)\tau} * Q(\tau) \end{aligned} \tag{10}$$

where we defined

$$Q(\tau) \equiv |q(\tau)|^2$$

. Then, we calculate the second moment of $\tilde{r}(\tau_{rt})$:

$$\begin{aligned} &\langle |\tilde{r}(\tau)|^2 \rangle = \\ &\int_0^{T_{rt}} \int_0^{T_{rt}} r(\tau_{rt}) r^*(\tau_{rt}{}') \langle R(\tau, \tau_{rt}) R^*(\tau, \tau_{rt}{}') \rangle d\tau_{rt} d\tau_{rt}{}' \end{aligned} \tag{11}$$

To continue we average over fiber realizations:

$$\begin{aligned} \langle \langle |\tilde{r}(\tau)|^2 \rangle \rangle_{\text{fibers}} &= \int_0^{T_{rt}} \int_0^{T_{rt}} \langle r(\tau_{rt}) r^*(\tau_{rt}{}') \rangle_{\text{fibers}} \\ &\qquad \cdot \langle R(\tau, \tau_{rt}) R^*(\tau, \tau_{rt}{}') \rangle d\tau_{rt} d\tau_{rt}{}' \\ &= \sigma_\rho^2 \int_0^{T_{rt}} \int_0^{T_{rt}} \delta(\tau_{rt} - \tau_{rt}{}') e^{-\tilde{\alpha}(\tau_{rt} + \tau_{rt}{}')} \\ &\qquad \cdot \langle R(\tau, \tau_{rt}) R^*(\tau, \tau_{rt}{}') \rangle d\tau_{rt} d\tau_{rt}{}' \end{aligned} \tag{12}$$

which leads to:

$$\langle \langle |\tilde{r}(\tau)|^2 \rangle \rangle_{\text{fibers}} = \sigma_\rho^2 \int_0^{T_{rt}} \langle |R(\tau, \tau_{rt})|^2 \rangle\, e^{-2\tilde{\alpha}\tau_{rt}} d\tau_{rt} \tag{13}$$

Hence, we obtain the final expression for the variance of the backscattered signal:

$$\begin{aligned} \langle \sigma_r^2(\tau) \rangle_{\text{fibers}} &= \int_0^{T_{rt}} \langle |R(\tau, \tau_{rt})|^2 \rangle\, e^{-2\tilde{\alpha}\tau_{rt}} d\tau_{rt} \\ &\qquad - e^{-2(\tilde{\alpha} + 1/|\tau_c|)\tau} * Q(\tau) \end{aligned} \tag{14}$$

III. Simulation

To test the theoretical model and the above formalism numerical simulations were performed. The simulation algorithm comprised a nested loop: an inner loop for running over different realizations of phase noise within an outer loop in

This article has been accepted for publication in IEEE/OSA Journal of Lightwave Technology. This is the author's version which has not been fully edited and content may change prior to final publication. Citation information: DOI 10.1109/JLT.2021.3138249

which the random fiber realizations were generated. The fiber was simulated as a vector of random complex backscatter coefficients, $\vec{h}$. The real and imaginary parts of the elements of $\vec{h}$ were uncorrelated zero-mean random variables with normal distribution. Their variances decay exponentially to represent the fiber's attenuation. The nominal detected complex field (at the absence of phase noise), after a roundtrip in the fiber, could be obtained by multiplying $\vec{h}$ with a convolution matrix, $\mathbf{V}$, whose columns were shifted versions of a single period of the interrogation signal. Matched filtering of the detected signal for its compression could be obtained by implementing $\vec{r} = \mathbf{V}^{\dagger}\mathbf{V}\vec{h}$. At the presence of phase noise, each element of $\mathbf{V}$, denoted as $\mathbf{V}_{n,m}$, was multiplied by an exponential phase term

$$\exp\left\{j\left[\phi_{n-m} - \phi_n\right]\right\}$$

where ϕ_n is the phase noise at the reference arm and ϕ_{n-m} is a delayed version of the phase noise which corresponds to the signal returning from a given position in the fiber. The phase-noise corrupted response following matched filtering is given by:

$$\tilde{r} = \mathbf{V}^{\dagger}\tilde{\mathbf{V}}\vec{h} = \mathbf{V}^{\dagger}\left[\exp\left\{j\left[\phi_{n-m} - \phi_n\right]\right\} .* \mathbf{V}\right]\vec{h}$$

where '$.*$' denotes element by element multiplication and $\tilde{\mathbf{V}}$ denotes the phase-noise corrupted convolution matrix. The phase noise sequence, ϕ_n, was generated via cumulative summation over a sequence of instantaneous frequencies, ν_n. The sequence ν_n comprised uncorrelated zero-mean normal random variables whose variances were chosen according to the desired linewidth to be: $\sigma_\nu^2 = \Delta\nu/(2\pi dt)$ where $\Delta\nu$ is the laser's linewidth and dt the simulation time step. Once $\tilde{r}$ was obtained it was possible to calculate the differential phase between positions separated by a given gauge length as well as $\langle|\langle\tilde{r}(\tau)\rangle|^2\rangle_{\text{fibers}}$ and $\langle\sigma_r^2(\tau)\rangle_{\text{fibers}}$ and to compare to the theoretical expressions (equations (10) and (14)) and the experimental results.

IV. Experimental Setup

Fig. 1 depicts the experimental setup used to validate the model. This is a conventional differential-phase OTDR sensor in which OPC coding was implemented. Two different lasers were used in the experiments: an NKT Koheras and an RIO Orion laser modules with nominal linewidths of 100Hz and 2kHz, respectively, according to test data provided by the manufacturers. In the setup, the output of the laser source is split into two branches. One branch is directly connected to the local oscillator input of a homodyne receiver that comprises a 90° optical hybrid and two balanced detectors. The other branch is fed to a Mach-Zehnder electrooptic modulator (MZ-EOM) that in the experiments is used to generate the OPC sequences, either LFM pulses or PPA sequences. For the generation of the PPA sequences, the MZ-EOM, which is of the standard push-pull type with opposite phase-shifts applied to the two arms of the interferometer, is biased at minimum transmission. This makes it generate BPSK modulation in response to the applied voltage [11]. The PPA sequence signal applied to the modulator is generated in an arbitrary waveform generator (AWG). For the generation of LFM

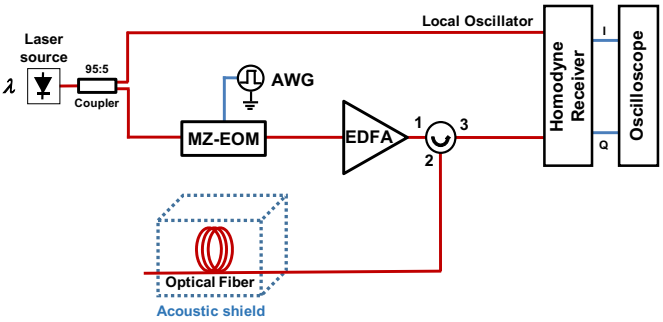

Fig. 1. Setup of the OPC ϕ-OTDR sensor used to experimentally validate the model.

pulses, the MZ-EOM is also biased at minimum transmission so that it generates optical double-sideband supressed-carrier (ODSB-SC) modulation. Then, sinusoidal modulation with a linearly increasing frequency is applied using the AWG so that two simultaneous LFM pulses are generated at each sideband. After homodyne detection, separated access to the two sidebands is readily available as the full optical field (amplitude and phase) is obtained, making it easy to filter out one of the sidebands via signal processing of the detected complex signal. The output of the MZ-EOM is amplified in an EDFA and launched into the sensing fiber. Finally, the backscattered signal from the fiber is detected in the homodyne receiver.

V. Results

A. Validation of the theoretical model

In order to validate the theoretical model, we conducted numerical simulations and experiments. Fig. 2 and Fig. 3 depict the calculation of the mean and the variance of the backscattered power along the fiber of the ϕ-OTDR in the setup for different laser sources, OPC types, and fiber lengths. In these figures, the theoretical model calculations are compared to those using the numerical simulations as well as to experimental measurements. In every case, good agreement is found, which confirms the validity of the simplified model introduced in section II. In these figures, the theoretical and numerical results assumed the nominal linewidth of 2kHz for the RIO laser, but 300Hz for the NKT laser, larger than the nominal value of 100Hz provided by the manufacturer. We attribute the need to use a higher linewidth for the modeling of the NKT laser to the experimental methods that are used to characterize this parameter in such a highly coherent laser, which are known to be ambiguous and challenging [24]. In any case, both values are close and of the same order.

As explained in section II, the theoretical mean and variance of the backscattered power is obtained by averaging over every possible realization of two random processes: the laser phase-noise and the configuration of scatterers in the fiber. In the experiments, obtaining multiple measurements for different phase-noise is relatively easy: just make sequential measurements and the laser source phase noise will be different for each of them. However, obtaining different fiber realizations is trickier since it would require using a multitude of different

This article has been accepted for publication in IEEE/OSA Journal of Lightwave Technology. This is the author's version which has not been fully edited and content may change prior to final publication. Citation information: DOI 10.1109/JLT.2021.3138249

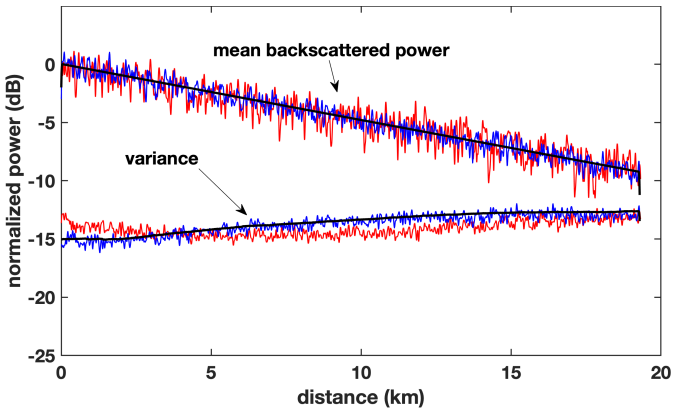

(a)

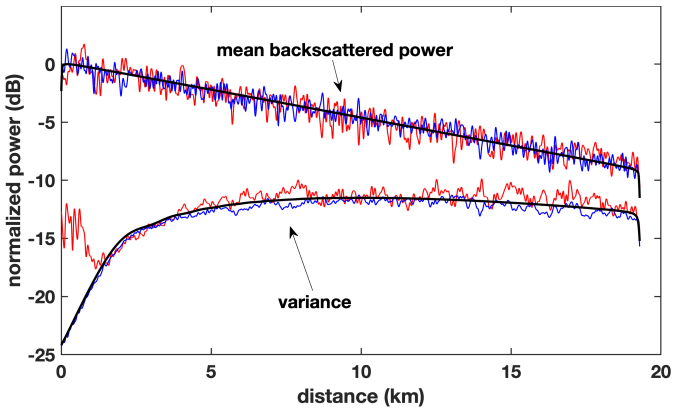

(b)

Fig. 2. Mean power and variance of backscattered signal along 19.3-km of G.652 fiber using the NKT laser and (a) PPA or (b) LFM OPC, calculated using theoretical (black), numerical (blue) and experimental (red) results.

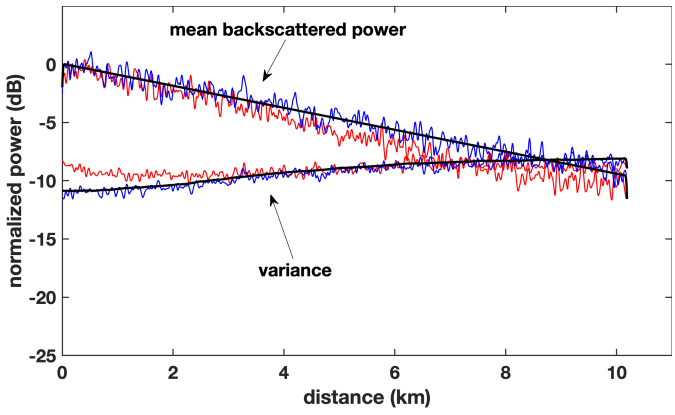

(a)

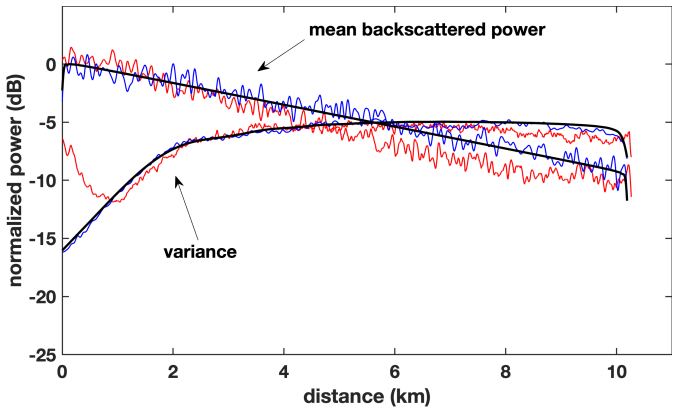

(b)

Fig. 3. Mean power and variance of backscattered signal along 10.2-km of G.652 fiber using the RIO laser and (a) PPA or (b) LFM OPC, calculated using theoretical (black), numerical (blue) and experimental (red) results.

fibers to perform successive measurements, which is not practical. Instead, we have adopted a different approach in which a single fiber was employed and the wavelength of the laser source was modified between measurements. This takes advantage of the fact that the Rayleigh backscattered signal can be regarded as statistically independent for pulses with optical frequency separation greater than the inverse of the pulse duration [25]. Therefore, what we did was to scan the wavelength of the laser source used in the setup using thermal tuning with small 0.5-nm steps. A total of 60 steps were used in the measurement in Fig. 2 and Fig. 3, which corresponds to an equal number of equivalent fiber realizations. At each step, a total of 32 successive PPA sequences or LFM pulses were launched to obtain an equal number of measurements with different phase-noise realizations. This number of wavelength steps and sequences was found to be statistically significant to get a reasonable convergence in the results. In addition, throughout the measurements, the fiber under test was placed in a special box for acoustic and vibration isolation.

The PPA code deployed in all measurements and calculations is a 331-bit code with an 800-ns bit duration, which gives a total of 264.8-μs duration for the sequence. This translates to a spatial resolution of 80 m after matched filtering. The motivation to choose such a moderate resolution was to reduce the number of samples required in the numerical simulations so that they took a reasonable amount of time. Notice that the objective of these experiments was not to demonstrate the enhanced spatial resolutions that are possible with OPC, which have been reported elsewhere [11], but to validate the theoretical model in section II. As for the LFM pulses case, the approach that we followed was to use a sequence equivalent to the PPA in performance. Hence, 264.8-μs pulses were used with a peak-to-peak deviation of the LFM of 1.25MHz, which gives a similar spatial resolution and coding gain to that of the PPA case.

As discussed in section II, our theoretical model considers just the phase noise term that represents noise with 'white' instantaneous frequency PSD. This is the term that is significant for the relatively fast phase dynamics that are associated with the differential-phase OPC ϕ-OTDR setup. However, other terms, particularly the 'flicker noise' term, are significant when longer time scales are involved. An example of this is when we calculate the mean of the backscattered power over a number of phase-noise and fiber realizations. As we have explained, the effect of the 'white noise' is just a reduction in the average backscattered power (see (10)), which is an important sensor performance metric. However, the presence of '1/f' noise translates into an additional slow 'drift' of the phase that does not have any practical effect on the differential-phase ϕ-OTDR sensor since the demodulated phases from

This article has been accepted for publication in IEEE/OSA Journal of Lightwave Technology. This is the author's version which has not been fully edited and content may change prior to final publication. Citation information: DOI 10.1109/JLT.2021.3138249

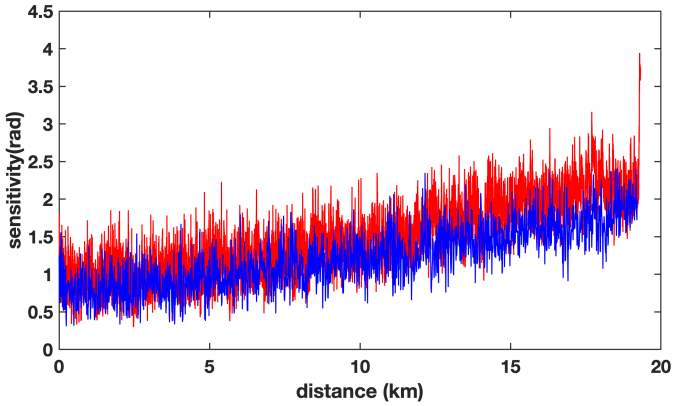

(a)

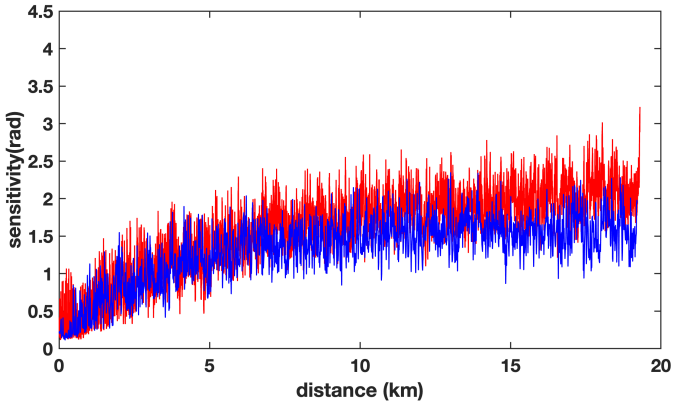

(b)

Fig. 4. Standard deviation of differential-phase measurements for a 19.3-km fiber using the NKT laser and (a) PPA or (b) LFM OPC, calculated using numerical (blue) and experimental (red) results.

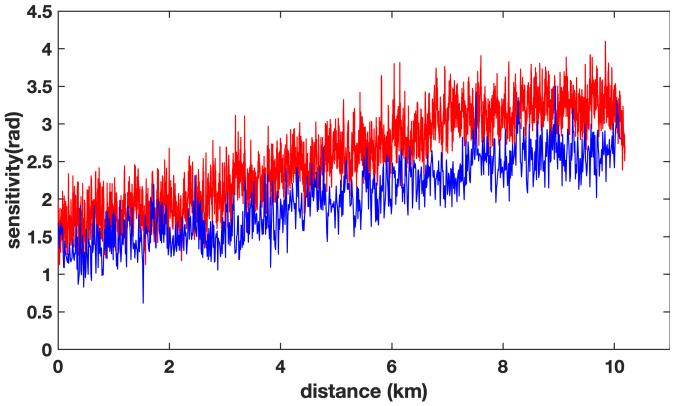

(a)

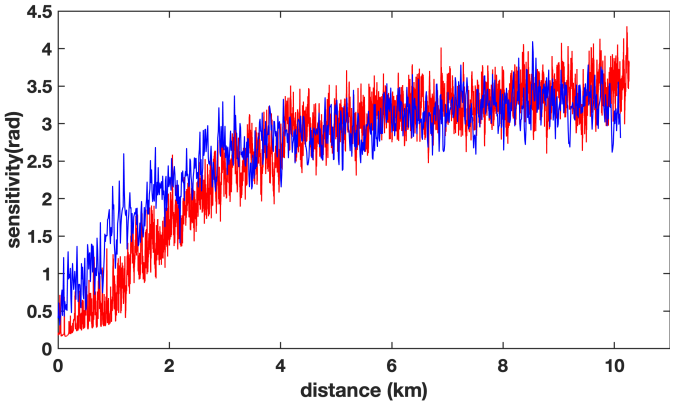

(b)

Fig. 5. Standard deviation of differential-phase measurements for a 10.2-km fiber using the RIO laser and (a) PPA or (b) LFM OPC, calculated using numerical (blue) and experimental (red) results.

nearby positions are equally affected by this drift. However, this slow phase drift needs to be removed in order to calculate the mean backscattered power from the experimental results because the method that is used to calculate this mean power is based on adding the responses for the different phase-noise realizations in complex form (amplitude and phase). In the absence of phase-drift, this gives the average response and from it the mean backscattered power is calculated. However, the presence of the phase-drift would lead to wrong results for the method and prevent us from easily assessing the experimental mean backscattered power that we intend to compare with the theory. The phase-drift removal can be done rather well for the measurements obtained with the NKT laser. The procedure that we devised was to retain for each measured signal after compression, just the higher amplitude locations, avoiding the fadings. The phase drift was then compensated using the values obtained using regression to the experimental optical phase measurements along the fiber. For the measurements with the RIO laser, the measurement was noisier as a result of its larger linewidth, this forced us to reduce the fiber length so as to have cleaner measurements that allow the application of the phase-drift compensation method. In both cases, it can be observed that after the application of the compensation method, the experimental measurements of the mean backscattered power along the fiber agree rather well with the theoretical and numerical calculations. Nevertheless, there is some divergence in the variance values at the start of the fiber. This is attributed to the limitations of the phase drift compensation method, which as any regression method has a limited precision that in this case manifests as a noise floor in the compensated measurement. However, as we move along the fiber, and particularly for the worst-case locations at the end of the fiber, the agreement in the variance is also very good.

Regarding the comparison of the use of OPC based on either LFM pulses or PPA BPSK sequences, observation of Fig. 2 and Fig. 3 shows that the evolution of the variance of the backscattered signal along the fiber is different for both cases; although, for the particular examples depicted here, at the end of the fiber their magnitudes relative to the mean backscatter power are very similar.

We also compared in Fig. 4 and Fig. 5 the standard deviation of the differential phase measurements obtained for the same phase-noise and fiber realizations as before. Notice that the noise in the differential phase measurement is really the important metric for the performance of a phase-measuring ϕ-OTDR sensor since it can be interpreted as its sensitivity, which is the term that has been used in the figures. The gauge length of these measurements was set equal to the spatial resolution although any other value can be used. Notice again

This article has been accepted for publication in IEEE/OSA Journal of Lightwave Technology. This is the author's version which has not been fully edited and content may change prior to final publication. Citation information: DOI 10.1109/JLT.2021.3138249

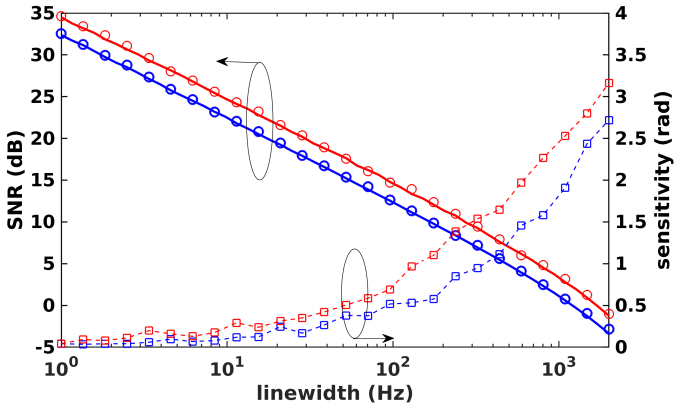

Fig. 6. SNR and sensitivity of differential-phase measurements versus linewidth at the end of a 10.2-km fiber using either PPA (red lines and symbols) or LFM (blue lines and symbols) OPC calculated using theoretical (solid lines) and numerical (symbols) results.

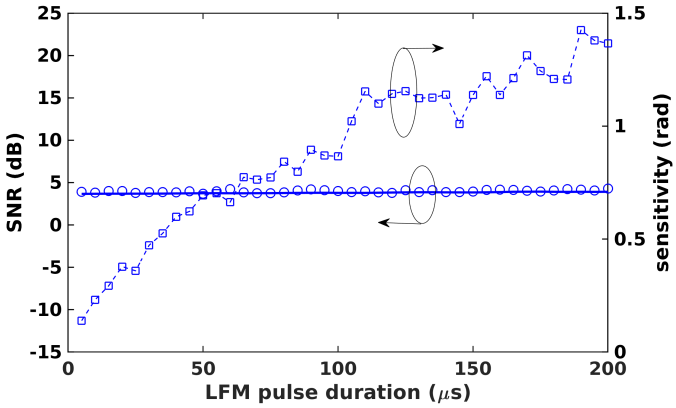

Fig. 7. SNR and sensitivity of differential-phase measurements versus sequence length at the end of a 19.3-km fiber using LFM OPC with a linewidth=300Hz and calculated using theoretical (solid line) and numerical (symbols) results.

that there is a very good agreement between the numerical calculations obtained from the theoretical model and the experimental results. This means that the presented model is valid to estimate the noise in the dynamic measurements used in differential-phase ϕ-OTDR sensors.

B. Dependence of sensor performance on laser phase-noise

Once the validity of the phase-noise model has been established, we now show preliminary results related to its application to optimize the performance of OPC ϕ-OTDR sensors. In the previous section, we have calculated the mean backscattered power and its variance in several configurations of the sensor. We can define an SNR metric as the ratio of these two magnitudes. However, as it is explained below, this SNR does not fully characterize the performance of OPC ϕ-OTDR sensors. This is in contrast to the case of non-OPC conventional ϕ-OTDR sensors, whose performance is limited by additive noise and where such 'static' SNR can be directly related to the sensitivity of the dynamic measurements [26]. Fig. 6 depicts calculations of the defined SNR and the measurement sensitivity at the end (worst-case location) of a 10.2-km fiber using the model presented in section II and deploying either PPA or LFM OPC with identical parameters to those in the previous section. Again the average of 60 fiber realizations each with 32 phase-noise realizations is shown. In addition, the calculated values are the average of the last 50 sampled positions at the end of the fiber. Notice that, as was expected, the SNR inversely depends on the linewidth. Also expected is that the larger the linewidth the worse the sensitivity obtained at the end of the fiber.

The model that we have presented also provides the capability to determine the optimum OPC parameters to use with a given system configuration. As an example, Fig. 7 depicts the SNR and the sensitivity for LFM OPC as a function of the length of the LFM pulse. This figure highlights the reason why SNR is not a useful parameter to characterize the performance of OPC phase-measuring ϕ-OTDR sensors. Note that, for a given linewidth of the optical source, the SNR is independent of the sequence length. However, it is apparent that the real performance metric of the system, the sensitivity, is enhanced as we reduce the LFM pulse duration. This is due to the nature of the effect that the laser's phase-noise has on the OPC. Eq. (10) conveys the fact that the average response from a given fiber location has two terms: one associated to the square of the sequence autocorrelation, which increases with the sequence length and provides the coding gain, and another exponential term that just depends on the fiber location and the coherence length of the source, but not on the OPC sequence duration. While not directly apparent from the formalism, Fig. 7 also suggests that the variance of the response also scales solely with the square of the sequence autocorrelation, at least in the case of the LFM. Therefore, the net result is that the SNR is independent of the LFM signal duration. However, the variation of the measured differential optical phase from a given location after OPC increases as the sequence experiences the laser's phase noise for a longer time. Another relevant observation is that the reduction of the sequence length as a means to enhance the sensor performance is just available with LFM but not with PPA OPC. The latter always requires a sequence length larger than the round-trip delay of the fiber [12], [11]. Therefore, PPA seems more suitable for systems with a shorter length of the fiber under test.

From the results depicted in Fig. 7, it would seem that OPC is not very useful, since the shorter the sequence length, and hence the smaller the gain provided by OPC, the better the sensitivity. However, that is not the case since in a real system there is an optimum sequence length at which the additive noise in detection starts to be the limiting performance factor instead of the noise in the measurement originating in the laser's phase-noise. This is highlighted in Fig. 8, where the experimental and theoretical sensitivities are calculated for an LFM OPC with 6-m spatial resolution. Note that both experimental and theoretical results display the same trend of enhancement with reduced pulse till a duration of around 30μs. From that optimum value, the experimental results show that further reduction of the sequence length just degrades the sensitivity. The divergence of the theoretical results for LFM pulse duration below the optimum and the

This article has been accepted for publication in IEEE/OSA Journal of Lightwave Technology. This is the author's version which has not been fully edited and content may change prior to final publication. Citation information: DOI 10.1109/JLT.2021.3138249

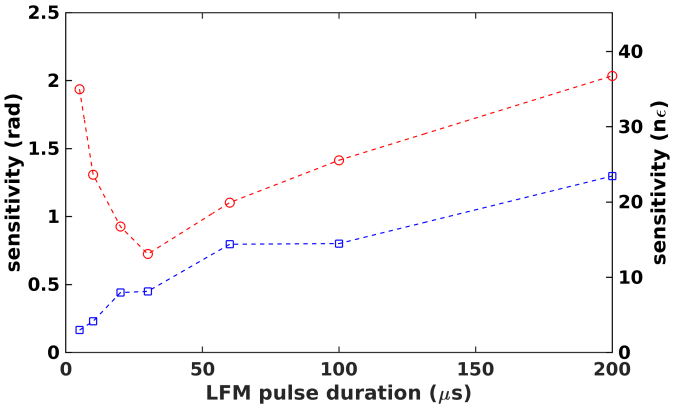

Fig. 8. Sensitivity of 19.3-km fiber under test using LFM OPC with 6-m spatial resolution. Numerical (blue) as well as experimental (red) results using the NKT laser are shown. Sensitivity is given in terms of differential phase as well as of strain.

small difference for larger values is due to the effects of additive noise, which is not included in the model. Note that for the optimum duration of the pulse in this example, the compression gain provided by LFM OPC compared to the use of single pulses is of $30\mu s/60ns = 500$. Finally, notice that in practical deployments of OPC, a technique for fading compensation such as frequency diversity would be applied to further enhance the system's sensitivity.

VI. Conclusion

In summary, we have introduced a theoretical model to quantify the effects of the phase noise of the optical source on OPC ϕ-OTDR sensors. Even though the ultra-narrow linewidth lasers typically used in these types of sensors have multiple phase-noise terms, we have demonstrated that just the 'white' instantaneous frequency PSD term is required to adequately model the effects that compromise their performance for dynamic measurements. This has paved the way for the derivation of closed-form expressions for the mean backscattered power and its variance along the fiber as well as for the implementation of simplified numerical simulations. Moreover, using the model, we have confirmed that, in most situations, the phase-noise of the laser is indeed the limiting factor to the performance of these sensor setups over other additive sources of noise such as optical or detection noises. This is in contrast to conventional non-OPC ϕ-OTDR setups in which phase noise tends to play a minor role when narrow-band sources are deployed because the differential-phase measurements of nearby positions mostly cancel out the common phase noise term. On the contrary, as the results in section V-B have shown, when using OPC, signal degradation takes place during the cross-correlation 'pulse compression' process and its severity depends on the round-trip delay to the reflection and the duration of the sequence (LFM pulse or PPA). Increased round-trip delay increases the decorrelation between the backscattered signal and the local oscillator used in the coherent detection, which translates to the detected signal. Increased duration of the sequence means that it experiences this decorrelated phase term for longer time, hence leading to an increased effect on the cross-correlation result.

Finally, we have demonstrated some preliminary application of the theoretical model to analyze and optimize the performance of a given sensor configuration. This has illustrated the capabilities of the model to answer basic questions about OPC deployment that remained unanswered until now, such as what is the optimum sequence or pulse duration to use for a particular ϕ-OTDR sensor configuration.

Acknowledgment

The authors would like to thank Enrique Piñeiro for his assistance in performing some of the experiments in this work, and Moshe Tur and Nadav Arbel for fruitful discussions. This work is part of the project PDC2021-121172-C21 funded by MCIN/AEI/10.13039/501100011033 and European Union "Next generationEU"/PRTR, and of project PID2019-107270RB, funded by MCIN/AEI/10.13039/501100011033 and FEDER "A way to make Europe". The work was supported in part by the Israeli Science Foundation (ISF), grant number 2675/20.

References

[1] A. Hartog, *An Introduction to Distributed Optical Fibre Sensors*, ser. Fiber Optic Sensors. Taylor & Francis Group, 2018.

[2] S. Liehr, L. A. Jäger, C. Karapanagiotis, S. Münzenberger, and S. Kowarik, "Real-time dynamic strain sensing in optical fibers using artificial neural networks," *Opt. Express*, vol. 27, no. 5, pp. 7405–7425, Mar 2019.

[3] L. Zhang, Z. Yang, N. Gorbatov, R. Davidi, M. Galal, L. Thévenaz, and M. Tur, "Distributed and dynamic strain sensing with high spatial resolution andlarge measurable strain range," *Opt. Lett.*, vol. 45, no. 18, pp. 5020–5023, Sep 2020.

[4] J. Pastor-Graells, H. F. Martins, A. Garcia-Ruiz, S. Martin-Lopez, and M. Gonzalez-Herraez, "Single-shot distributed temperature and strain tracking using direct detection phase-sensitive otdr with chirped pulses," *Opt. Express*, vol. 24, no. 12, pp. 13 121–13 133, Jun 2016.

[5] W. Zou, S. Yang, X. Long, and J. Chen, "Optical pulse compression reflectometry: proposal and proof-of-concept experiment," *Opt. Express*, vol. 23, no. 1, pp. 512–522, Jan 2015.

[6] S. Wang, X. Fan, Q. Liu, and Z. He, "Distributed fiber-optic vibration sensing based on phase extraction from time-gated digital ofdr," *Opt. Express*, vol. 23, no. 26, pp. 33 301–33 309, Dec 2015.

[7] B. Lu, Z. Pan, Z. Wang, H. Zheng, Q. Ye, R. Qu, and H. Cai, "High spatial resolution phase-sensitive optical time domain reflectometer with a frequency-swept pulse," *Opt. Lett.*, vol. 42, no. 3, pp. 391–394, Feb 2017.

[8] D. Chen, Q. Liu, and Z. He, "Phase-detection distributed fiber-optic vibration sensor without fading-noise based on time-gated digital ofdr," *Opt. Express*, vol. 25, no. 7, pp. 8315–8325, Apr 2017.

[9] J. J. Mompó, S. Martín-López, M. González-Herráez, and A. Loayssa, "Sidelobe apodization in optical pulse compression reflectometry for fiber optic distributed acoustic sensing," *Opt. Lett.*, vol. 43, no. 7, pp. 1499–1502, Apr 2018.

[10] C. Dorize, E. Awwad, and J. Renaudier, "High sensitivity φ -otdr over long distance with polarization multiplexed codes," *IEEE Photonics Technology Letters*, vol. 31, no. 20, pp. 1654–1657, 2019.

[11] J. J. Mompó, L. Shiloh, N. Arbel, N. Levanon, A. Loayssa, and A. Eyal, "Distributed dynamic strain sensing via perfect periodic coherent codes and a polarization diversity receiver," *J. Lightwave Technol.*, vol. 37, no. 18, pp. 4597–4602, Sep 2019.

[12] L. Shiloh, N. Levanon, and A. Eyal, "Highly-sensitive distributed dynamic strain sensing via perfect periodic coherent codes," in *26th International Conference on Optical Fiber Sensors*. Optical Society of America, 2018, p. TuE25.

[13] M. Sagues, E. P. neiro, E. Cerri, A. Minardo, A. Eyal, and A. Loayssa, "Two-wavelength phase-sensitive otdr sensor using perfect periodic correlation codes for measurement range enhancement, noise reduction and fading compensation," *Opt. Express*, vol. 29, no. 4, pp. 6021–6035, Feb 2021.

[14] S. Wang, W. Zou, X. Long, and J. Chen, "Influence of phase noise on measurement range in optical pulse compression reflectometry," in *2015 Opto-Electronics and Communications Conference (OECC)*, 2015, pp. 1–3.

[15] E. Awwad, C. Dorize, S. Guerrier, and J. Renaudier, "Detection-localization-identification of vibrations over long distance ssmf with coherent $\delta\phi$-otdr," *Journal of Lightwave Technology*, vol. 38, no. 12, pp. 3089–3095, 2020.

[16] O. H. Waagaard, E. Rønnekleiv, A. Haukanes, F. Stabo-Eeg, D. Thingbø, S. Forbord, S. E. Aasen, and J. K. Brenne, "Real-time low noise distributed acoustic sensing in 171 km low loss fiber," *OSA Continuum*, vol. 4, no. 2, pp. 688–701, Feb 2021.

[17] S. Norimatsu and O. Ishida, "Impact of flicker noise and random-walk noise on a phase-locked loop with finite propagation delay," *Journal of lightwave technology*, vol. 12, no. 1, pp. 86–95, 1994.

[18] A. Godone, S. Micalizio, and F. Levi, "Rf spectrum of a carrier with a random phase modulation of arbitrary slope," *Metrologia*, vol. 45, no. 3, p. 313, 2008.

[19] M. Fleyer, J. P. Cahill, M. Horowitz, C. R. Menyuk, and O. Okusaga, "Comprehensive model for studying noise induced by self-homodyne detection of backward rayleigh scattering in optical fibers," *Optics express*, vol. 23, no. 20, pp. 25 635–25 652, 2015.

[20] A. Kakkar, J. R. Navarro, R. Schatz, X. Pang, O. Ozolins, A. Udalcovs, H. Louchet, S. Popov, and G. Jacobsen, "Laser frequency noise in coherent optical systems: spectral regimes and impairments," *Scientific reports*, vol. 7, no. 1, pp. 1–10, 2017.

[21] M. O. Sahni, S. Trebaol, L. Bramerie, M. Joindot, S. P. Ó. Dúill, S. G. Murdoch, L. P. Barry, and P. Besnard, "Frequency noise reduction performance of a feed-forward heterodyne technique: application to an actively mode-locked laser diode," *Optics letters*, vol. 42, no. 19, pp. 4000–4003, 2017.

[22] E. Fomiryakov, D. Kharasov, O. E. Nanii, S. Nikitin, and V. N. Treshchikov, "New approach to laser characterization using delayed self-heterodyne interferometry," *Journal of Lightwave Technology*, 2021.

[23] J. A. Armstrong, "Theory of interferometric analysis of laser phase noise∗," *J. Opt. Soc. Am.*, vol. 56, no. 8, pp. 1024–1031, Aug 1966.

[24] L. Zhang, L. Chen, and X. Bao, "Unveiling delay-time-resolved phase noise statistics of narrow-linewidth laser via coherent optical time domain reflectometry," *Opt. Express*, vol. 28, no. 5, pp. 6719–6733, Mar 2020.

[25] M. D. Mermelstein, R. Posey, G. A. Johnson, and S. T. Vohra, "Rayleigh scattering optical frequency correlation in a single-mode optical fiber," *Opt. Lett.*, vol. 26, no. 2, pp. 58–60, Jan 2001.

[26] H. Gabai and A. Eyal, "On the sensitivity of distributed acoustic sensing," *Opt. Lett.*, vol. 41, no. 24, pp. 5648–5651, Dec 2016.